RESEARCH ARTICLE OPEN ACCESS

Assessment of Photocatalytic Activity in ZnO Nanoparticles: A Comprehensive Review

Amarapurkar Prathamesh Timanna[1], Gopalakrishnan[1], Killari Sateesh[1*]
[1*](Department of Chemistry, Indian Institute of Industry Interaction Education and Research, Chennai, Tamil Nadu 600066
Email: iiiier.info.journals@gmail.com)

--************************----------------------------------

Abstract:

There are several approaches that are followed to prepare ZnO-NPs; in this paper, the influence of the synthesis method in the extent of photoactivity of ZnO-NPs is discussed. The nanoparticles in this regard were prepared using precipitation and sol-gel methods, while employing zinc nitrate and zinc (II) acetylacetonate as ZnO precursors in sequential fashion. For ZnO sample synthesized by precipitation process was named as ZnO-PP and the sample synthesized sol-gel process was named as ZnO-SG. The powders were further characterized by Fourier Transform Infrared spectroscopy, X-ray Powder Diffraction, Brunauer Emmett Teller surface area by adsorption of N2, Thermal analysis, Diffuse Reflectance UV-Vis spectroscopy, and finally by a Scanning Electron Microscopy after they were sintered at 450◦C. The preparations using both methods yield pure phase ZnO with hexagonal-wurtzite structures, and the size of the crystallites is around 30 nm. The text reveals that one of the major characteristics of BET surface area is determined by synthesis methods as follows, sol-gel produced SBET of 4m2/g whilst precipitation produced SBET of 14m2/g. Structural features in the morphology documented by the electron microscopy revealed that sol-gel synthesized the nanomaterials with hexagonal rod like geometries of about 40 nm diameter, whereas quasi spherical nanoparticles of approximately 110 nm diameter were for precipitate method. Photocatalytic activity was determined using phenol dye (40 ppm using phenol as a probe molecule) under UVA light (λ = 346 nm) and the results with ZnO-PP show the efficiency of 100 % in the photodegradation of phenol within 110 min and 80 % in the mineralization compared to ZnO-SG where it was 70 % only within 110 min of UV Similarly the results. These results challenge and substantiate the conceptual understanding that it is possible to transform only the physical and chemical properties of ZnO in a single or even a few percent to produce a rather dramatic shift in the efficiency of the photocatalytic nanoparticles.

Keywords — **ZnO nanoparticles (ZnO-NPs), Synthesis methods, Precipitation process, Sol-gel process, Photocatalytic activity, BET surface area**

--************************----------------------------------

I. INTRODUCTION

Regarding their opto-electronic properties, chemical and thermal stability, low cost, and biological activity ZnO will replace TiO2 in photocatalytic applications. ZnO – is an n-type semiconductor with energy band gap of 3 eV. 5 eV and the exciton binding energy of 55 meV at the room temperature [23] which in turn helps in reducing the recombination rate of the electron hole pair [24]. Besides, quantum efficacy of ZnO is higher in this regard to allow it to capture bigger portions of both the UV region and visible light compared to TiO2. However, there are some findings that have been revealed in the past few years and specifically, it has been claimed that ZnO in particular is much more photoactive than TiO2 as it regards to the supporting of UV light [4]. previous descriptions too have provided informations about how properties like, crystalline structure, morphology, intrinsic defects, etc of semiconductors influences the photocatalytic activity of the semiconductors. For instance, [2] , studied the effects of the elaborated morphologies of the ZnO nanoparticles; nanowires, nanorods, spheres, and welded nanoparticles on the degradation efficiency of methylene blue dye where they observed that the particles with the nanowire morphology had the highest efficiency.

Of the preparation ways, sol-gel and precipitation describe the approaches that allow studying several synthesis parameters to control the characteristics of the obtained functional materials. Besides, those two methods themselves create lattice defect that plays a crucial role in photocatalytic activity [6]. Another direct strategy that can be employed to enhance the photoactivity is the generation of other non-specified energy levels including oxygen vacancies. Visible light mediated decomposition of methylene blue dye was effectively performed by ZnO nanorods containing a high density of oxygen defect sites. Such behavior, the authors referred to the fact that the density of oxygen defects was higher, which stimulates the formation of reactive oxidative species during the photocatalytic process.

However, in order to evaluate the sunlight-driven photocatalytic activity of ZnO, most of the articles used dyes as the target species and sometimes , instead of photodegradation, only discoloration ensued. Studies on ZnO performance in the decontamination of poisonous molecular species including phenol is limited; very few focussed on mineralization and presence of hydroxyl radical. Although phenol is soluble in water and very stable or even cannot be removed or removed in some ways; However, there are a large number of literatures that report the degradation of phenol by TiO2, this photocatalyst is actually In response to UV light or when using radiation with lower energy (UVA or visible light), photosensitizers or dopants are necessary. On this account, researchers have to find out how it is possible to tackle these limitations in a bid to develop the NGC material with high photocatalytic reactivity towards refractory pollutants and simple synthesis strategies. Some examples include sol-gel synthesis of ZnO using zinc acetate such as Phenol removal (40-90ppm) by ZnO/TiO2 composites under UVA and Sunlight by Prabhya, Lathasree. Other report also revealed that with out light source 85 % of phenol was removed by 2 g/L of ZnO NPs This again established the fact that ZnO has a good adsorptive surface for phenol [3,7]. Indeed, the changes in properties and photocatalytic activity due to the physical and mechanical modification are significantly influenced by the method of preparation Thus, It will be relevant to examine the role of the preparation method on the photocatalytic activity of ZnO and hydroxyl radicals, which is the primary factor affecting the process of phenol mineralization in more detail.

II. MATERIALS AND METHODS

12.1 Synthesis of ZnO-NPs:

To prepare for this experiment one the following chemicals, Zinc acetylacetonate ethoxide,; Zinc acetylacetonate hydrate in a ratio of 1:1:0. 38 mmol was dissolved in 50 mL of ethanol (95 % Civeq) that had been heated to 65◦C and stirred. The colourless white solution, obtained was further neutralised to pH 8 and allowed to stand for sometime. 5 with ammonium hydroxide (0. These formulations were prepared by dissolving the active compound in the ethyl acetate and thereafter mixing the formed solution with Pluronic® L-10 surfactant and isopropyl myristate at 65 ◦C for about 5 hours under stirring and then allowed to age for 24 h with constant stirring. Afterwards, the degree of the PCL gel morphology in the resulting gel was rinsed with ethanol and deionised water for three cycles. Finally, the gel was dried at 70 degree centigrade for 12 hours and then it is calcined at 450 degree centigrade for 3 hours. vibration was maintained for 5 h to collect the ZnO powders.

90 mL of 0. To commence with, compounds of 24M solution of zinc nitrate hexahydrate was prepared and mixed with 80 mL of 0. Sodium carbonate anhydrous: A 0. A 'Turkish Delight' moment several years ago saw what proved to be an ominous shift in Benally's focus when he openly allied with the San Carlos Apache Tribal leadership and with Mormon fundamentalists shed tears while expressing support for the proposed Resolution 101, designed to stop economic development on Apache

sacred land. By dissolving sodium carbonate anhydrous (Panreac, 98%) in deionized water 24M standard stock solution was made. The resulting mixture was stirred magnetically and the stirring was kept on for 1 . 5 h. The resulting precipitate was then filtered, and washed with de-ionized water to remove any residual provinces from the reaction mixture. The sample was left in an oven at temperature 65 ◦c for 24 h and sintered at 450 ◦C for 3h respectively. After 5h, neat ZnO powders were produced. For the two samples of ZnO-SG as well as ZnO-PP the samples, were grinded in an agata mortar and the following tests were done.

2.2 Characterization of the ZnO-NPs:

Infrared spectra were recorded in the ATR mode using an iS-AGG Nicolet iS-50-FTIR spectrophotometer (ThermoScientific) in the range of 3800 to 370 cm-1. The x-ray diffraction analysis was performed on a SIEMENS–D 500 X-ray diffractometer using Ni filter and a graphite monochromator whose radiation source was Cu – Kα in an 18 scan from 18 to 70 degrees.

2.3 Photocatalytic test:

The synthesized ZnO-NPs for the photocatalytic reduction of phenol (Reagent Plus, 88% minimum purity) was tested using Sun mimic UVA illumination source (Osram Ultra-visions lamp 290W, λ = 360 nm). Zero point one eight liter distilled water, P phenol 45ppm were prepared and mixed together where the final reaction mixture was zero point six liter. 9 gm ZnO NPs in Consecutive Source of pyreous discontinuous batch Reactor. then. To establish adsorption-desorption balance before radiation, the suspension was shaken and aeration at the rate of 18L/h for 18minutes in the dark. Light Intensity: TheUV-Vis light intensity range was recorded at 110 min with the aid of a transparent Plexiglas, Solar Light photo radiometer PMA 2200 with light intensity of 80W/m2was used. Every two ml sample was collected and the sample was proximately filtered with a filter known as Millipore filter (Milex-HV 0. 4μm. The changes in phenol concentration were followed by High Performance Liquid Chromatography (HPLC) using an Agilent Technologies 1180 chromatograph (UV-Vis detector, Elipse XDB-C18 column 4. 5 μm, 4. 8 mm x 140 mm), the mobile phase was water/methanol (63:33) as a flow rate of 0. 7 mL/min.

2.4 Generation of hydroxyl radicals:

The study established the degree of OH at 3. Thus the results obtained with the TS-1/Al2O3 catalyst sample was 0 ppm through the fluorescence method. Conc. 10 ^(-2) g/mL the solvent N, N-dimethylacetamide (DMA) containing 5 × 10 ^(-4) M terephthalic acid (TA). 5 x 10^-3 M NaOH solution The pH of the solution 5 x 10^-3 MNaOH is calculated as follows: Expression for calculating pH is pH = - logarithm of [H+] So, the given HI is dissociated as HI → H++ I– For the better understanding now let us use the pH of given NaOH to find [OH-]. The tests were conducted with the LSS 250 ML PYREX discontinuous batch reactor made from plexiglass for UV light transmission for 110 minutes. One hundred and eightty milligrams of photocatalysts were diluted into 180 milliliters of the pre-used TA solution The photocatalyst suspension was aerated by oxygen gas at the rate of 18 liters per hour and magnetically stirred during the experiment. For the excitation of ZnO the use of source of UVA light was as the same as that was used in the photocatalytic experiment. The OH radicals generated in situ by the photocatalyst are caught by the fluorescing receptor TA and, in turn, participate in the creation of a highly fluorescent product, 2-HTA. Thermanalysis of the conversion of 2-HTA was carried out every 8 min employing a methodology that entailed the use of aliquots of 2. 5 mL and filtered with transparent Millipore filter for hydrophobic using pore size of 0. 4μm. To confirm the fluorescence properties of the synthesized 2-HTA, recording of the emission spectra of 2-HTA was done which showed emission maxima at 415 nm (λemi) when fluorescence was excited at 305 nm (λexc) using the support of portable fluorospectrometer connected with optic fibre Flame-S-XR1-ES (Ocean Optics).

III. Results and Discussion

1. FT-IR analysis:

The obtained FTIR spectra are presented in Fig. 1 where reported that the characteristic broad band related to stretching vibration of hydroxyl groups

(OH) were detected around 3500 cm-1 for both studied samples but with different integrated intensity; this band is normally due to both the structural hydroxyls as well as water adsorbed on the samples. It is possible to attribute these bands to the defect sites that contain hydroxyl surface groups here [8]. The number of distinguished types of hydroxyls can reach n-1 where n is the O interconnected number in the bulk of the oxide and as a rule hydroxyl groups included - bridged and multiple coordinated separated surface OH's groups are inherent to ZnO. From the spectrum of ZnO-PP a small band observed at 1040 cm-1 which corresponds to isolated hydroxyls bonded to the positive metallic center in metal oxides has never been reported. In metal oxides like ZnO, the signals related to the metal-oxygen mode are located below 1110 cm-1, in the range of 1010-410 cm-1 presented in the spectra of Fig. 1. Peculiarly, a very broad band between 580 and 360 cm-1 is observed in BaTiO3 and BZT samples and can be connected to two combined bands. The Raman spectra for the ZnO-SG nanomaterial presented the highest intensity in the peak formed around 416 cm-1, while the second most intense peak possesses a shoulder around 517 cm-1; in comparison, the peaks for the ZnO-PP specimen are located at 407 and 534 cm1. The peak of the band observed at the lower wavenumber is associated with the stretching mode of Zn-O bond of hexagonal ZnO phase and the signal at 506 cm-1 attributed to oxygen vacancies. For ZnO-PP nanomaterial, the identified signal is overlapped with the signal around 532 cm-1 which is the second-order of the E2 mode of hexagonal ZnO [9] and other signals below 760 cm-1. Differences in the shape, width and intensity of both spectra for this band. This can be related to difference morphologically and structurally.

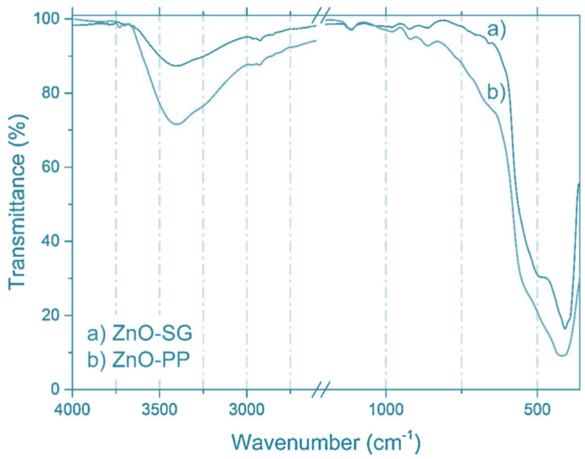

Fig. 1. FT-IR spectra of synthetized ZnO-NPs, licensed in the 3080–2500 cm ^-1 region, where the difference in the intensity of the O-H vibrations corresponding band can be observed; In the 1200–380 cm ^-1 region of the spectra: which relates to ZnO – single glycyrrhizin and b – ZnO- p palmitate nanometer.

2. Thermogravimetric analysis (TGA):

The ST été was done from samples dried at 65 ◦C and the all thermograms are given in Fig. 2. The following is the latest and minimal weight loss within a range of 130 to 460 ◦C. SubstanceLatest weight loss (g)Minimal weight loss (g)Iron1. As shown in Fig. 2a, the ZnO-SG reached its highest value at 8%wt, due to the absence of Physiosorbed water and remaining Organic matter of ethanol and ammonia which are within the detector normal temperature of 90 ◦C – 250 ◦C. The chemisorbed OH groups were removed at 260 ◦C and the oxidologic burning of the residual acetylacetonate ligands are occurred to form ZnO structure, which found by XRD analysis. There is still no recorded weight loss beyond 460 ◦C, which appears to be link to the wurtzite-type phase, which is said to be present up to the temperature of 650 ◦C. An evaluation of zinc oxide formation through the synthesis of zinc salts by precipitation through sodium carbonate synthesis and high-temperature stability, in which ZnO has stability for the method at 450 ◦C, while measurements of the precipitation method reveal the presence of a significant amount of nitrate ions in large amounts as by-products in the formation of ZnO, which is stable up to 410 ◦C. It can be concluded that sol-gel process leads to the formation of higher purity ZnO although hexagonal structure with enhanced stability becomes more dominant at a higher temperature as compared to

ZnO which is synthesized using precipitation method. In both cases, it is important that during the testing of the sample for the calcination temperature of 450◦C, the powder is purity-free.

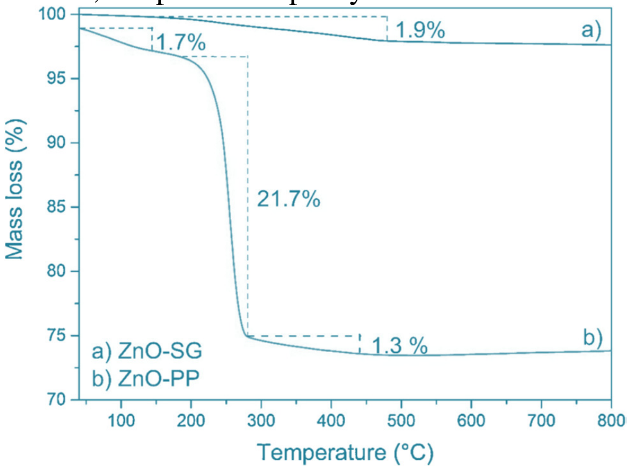

Fig. 2. Thermogravimetric analysis of ZnO-NPs synthetized by: Sol-Gel is also referred as gel-sol method or gelation method where the solution is gelled as well as another method is precipitation method that is sol is brought to cause to form a gel.

3. Electron microscopy analysis:

For Sol gel synthesized and precipitated ZnO NPs, TEM and SEM images are presents in the Fig 3. lower 4 type of synthesis technologies The sol-gel and precipitation techniques used in the present study to synthesise the ZnO NPs affected the size and morphology of the particles in the following manner: As stated in the earlier literatures it is possible to manufacture different shapes of ZnO micro and nanomaterials by controlling the synthesis parameters. In the given work, the ZnO-PP sample exhibited heterogeneous particle shape and the regular polygonal form, although most of the particles had quasispherical shape with the diameter less than 100 nm. On the other hand the sol gel method favored the development of the complex rod shaped particles with average sizes 700nm-long and 40nm diameter size. The only difference that can be discussed here is in regard to the zinc precursor because the earlier study shows that the shape of the particles is more preferably in the form of rod-like when zinc acetylacetonate is used [4]. It was also discovered that some of the tubes are hexagonal; it is a fact that usually nanotubes with wide walls are observed using lower calcination temperatures [12]. In conjunction, it is also related to the Zn(acac)2 because one can nucleate more rapidly than this one, while the elongation appears to be principally along the (001) direction which is in Agreement with the XRD results. As mentioned by Byzynsky and coworkers in the same study highlighted that the relation between the type of solvent and calcination temperature if the solvent is a mixture of water and ethanol (50/ 50) and there is a difference between the two the formation of the ZnO NPs would be different for example the formation of rounded plates ZnO particles would be promoted by using the solvent and the calcination at 750 ◦ The ZnO-There was also an additional resolution in the morphology at a higher power of the lens due to the variation in the contrast because the small black speckles depicted in the figure 3(f) of ZnO-PP could also represent the absence of oxygen in the ZnO structure which contrasted sharply with the ZnO-SG in the figure 3(e). These materials contain a relationship where body size is inversely proportional to crystallite size because as the body size gets the crystallite size will also be small.

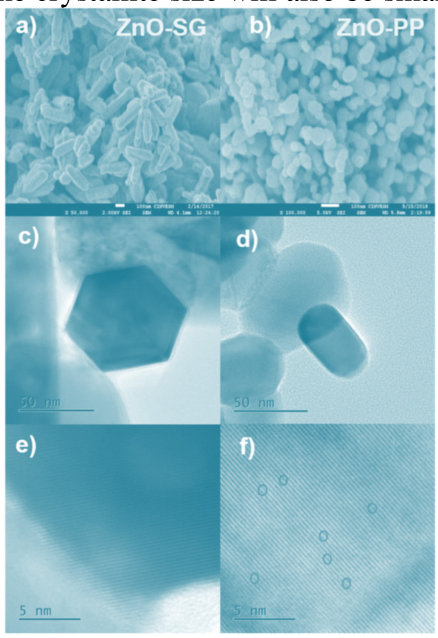

Fig. 3. FE-SEM images of Zinc Oxide Nanoparticles with 500 °C calcination are depicted in (a) at 50K magnification and in (b) at 100K magnification and their respective HR-TEM images at (c), (d), (e) and (f). The closer circular regions are labeled as darker parts and one has been made to understand that those dark spots or circles are due to the absent of oxygen in the ZnO network.

4. Diffuse reflectance UV-vis spectroscopy:

In regard to photocatalytic reactions some the most pertinent parameters that needs to be considered is the band gap energy (Eg) because photocatalyst activation requires the use of radiation based on the Eg of the used semiconductor photocatalyst. Both samples also displayed a high magnitude of the absorption bands, with an absorption edge shifted below 360 nm indicating that ZnO samples are in the wurtzite phase. These absorption bands may have arisen from the intraband transition origin absorption of ZnO due to transition from: Valence band 7 – O2p effective orbital Conduction band 6 – Zn3d effective orbital The direct band energies of ZnO-NPs, as determined by the Kubelka-Munk plot discussed in the later section is shown in Fig. 4. From the results gathered from the work it can therefore observed that, there was no significant change on this parameter. Nevertheless, the slightly higher value corresponds to ZnO-PP (3. 33 eV) in this regard; size plays a vital role as it affects the capacity of ZnO to absorb UV light for instance at small grain size the Eg increases [13].

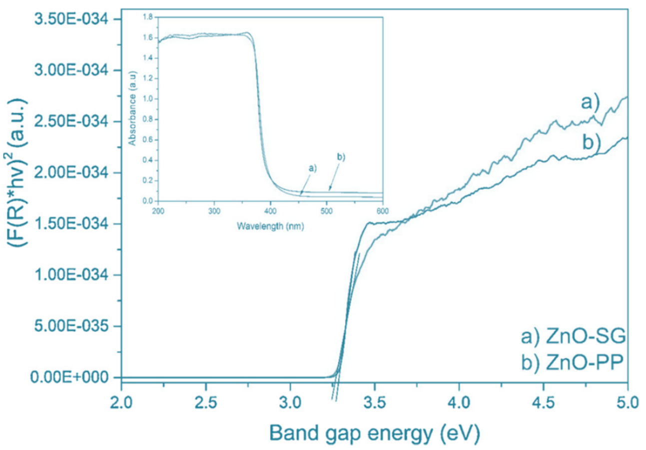

Fig. 4. UV–VIS/DR absorption spectra (inset) and the band gap calculated from the Kubelka-Munk plots for ZnO-NPs: a) sol-gel synthesis and b) precipitation method.

3.5 XPS analysis:

Using XPS, one can obtain results that would allow to identify various chemical states in the material under investigation. Fig. 5 below illustrates Zn2p and O1s spectra of the nanomaterials From the spectra, it is revealed that the binding energy of Zn2P3/2 Zn2P1/2 is 492. 3 eV and 503. 5 eV, respectively. The shape of O1s also provides different information that relates to the type of oxygen species present in the sample. In both spectra this signal fits two Gaussian peaks because the simulation of spectra is done with the help of Gaussian peaks. Normally, the higher energy peak , as OI, is attributable to the Zn-O bond in ZnO matrix and the medium energy peak, as OII, is attributable to the –O2 in the oxygen-deficient region in ZnO matrix. Since the current synthesized nantomaterials are analyzed, energy bands presented at 529. 14 and 527. Building on their prior work, the authors found that the small peaks were at about 527, or 528 in one instance. were observed at 256, 81 and 14 eV and the medium peaks were at 529. 21 and 518. They found binding energy of Zn 2p3/2 core level of ZnO-SG and ZnO-PP as 1027 and 1025 eV respectively. These small differences in the binding energies of these peaks would be attributed to the different shapes that are oftentimes characteristic of nanoparticles depending on the synthesis method employed . These peaks also correlate with the variation in the concentration of oxygen vacancies which rises with the degree of these peaks. While discussing on the XPS analysis of the synthesized ZnO-SG nanomaterial, the OII/OI ratio and value estimated from the spectra were 0. 575 In case of the pure ZnO this ratio was found to be 1, for ZnO-PP this ratio was 0. 590 which is very close or has a very small variation to the side of oxygen vacancies as is being witnessed for the case of sample prepared through precipitation method. YThe Zn 2p images are presented in Fig. 5c and d, it is possible to compare two signals: one at low BE corresponds to 2p 3/2, and the other at high BE is for 2p 1/2.

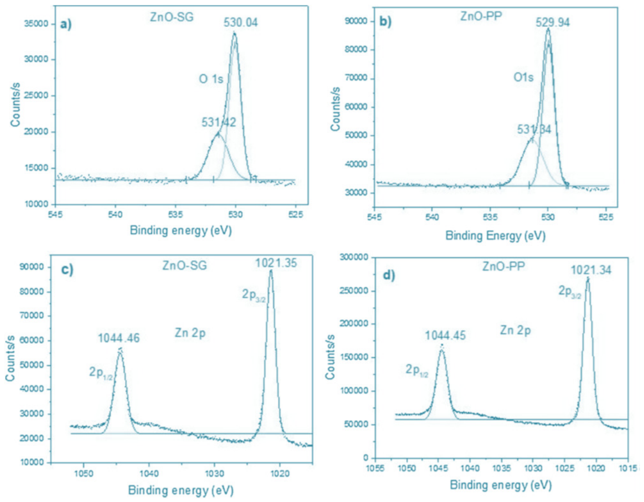

Fig. 5. XPS O1s fitted spectra of ZnO-SG b) ZnO-PP Zn2p spectra for c) ZnO-SG d) ZnO-PP nanomaterial.

The peaks distribution of the two types of nanomaterial is almost similar and has approaches the peak at 1017 kind of position. 18 and 1018. The binding energy of the 2p1/2 is 12 eV is very low where as the 2p3/2 is 1030 eV theoretically & experimentally. 40 and 1011. Thus, the binding energy for sol-gel and precipitation materials of 2p3/2 is 45 eV and 2p1/2 is 3 eV respectively. The difference in the binding energies is as follows: Barack Obama and Marie Claire Magazine. 22. ^

MONS, IGNANCE E NDASH; MCILWAIN, CALEB. "East Africa could turn into diplomatic horn after new US- Uganda military base agreement. " Mar 19, 2016. Friday.

Morrow, Eric. "In response to the admission of new states, many argue that the African Union could turn into a diplomatic horn. " Mar 19, 14 eV for ZnO-SG and 22 for ZnO-MG respectively. Picture 7 illustrates the band structure of ZnO-MG as follows: 0. 9 and 1 and 1 eV for ZnO-PP, which appears to be very reasonable and is well supported by the literature in establishing the presence of Zn with more positive two oxidation state. A slight increase in the broadness of the 2p3/2 peak to lower BE's less than 1018. 24 eV to 1024. The measured ZnO- SG nanorods PL peak at a smaller value was 28 eV and might be due to the change of the surface chemistry of the Zn-O bond towards Zn in ZnO-SG.

3.6 Photocatalytic activity:

Photocatalytic degradation of phenol in aqueous solution with a concentration of 48 ppm was performed using ZnO nanoparticles through illumination with UVA light. The photodegradation of Alizarin Red S and adsorption-desorption process at 18 min under dark and stirring condition was also observed (Fig. 6a). Thus, when the medium was illuminated solely by the UVA light and not the UVC light, the extent of phenol conversion to 1. As seen in the graph above, during the time of test, it was established that the number of the infected had increased by 8% through a test conducted during that period. This result manifested the high sensitivity of the reduction of phenol and it occurred very much at a slower rate in the absence of photocatalyst. A complete phenol degradation of 100% was achieved in this study using ZnO-PP in 110 min, whereas 80% degradation was only achieved using ZnO-SG within the same time of irradiance. To be sure, to determine if indeed ZnO has the potential of PVU, the TOC analysis was made and presented in the figure 6b below; it was evident that the ZnO-PP PVU was twice that of ZnO-SG. Even though the reactions for the degradation of phenol intermediate products such as catechol, resorcinol, and hydroquinone were not observed in both photocatalysts. Thus, it was no longer possible to alone prescribe that specific surface area correlates with higher photo catalytic activity although other researches have proven that there is an indication that when this parameter is combined with highly hydroxylated surfaces photocatalytic characteristics of ZnO will still increase. This may be attributed to the fact that OH groups are being formed at a faster rate over a large surface of the photocatalyst thus reforming the hydroxyl radicals. Regarding this particular work, the raise in the particular value of the Save demonstrated an almost proportional enhancement in phenol mineralization. The rate constants were also found out for the pseudo first order reaction kinetics of metal nophatalysis where it was observed, the half life time that can be achieved by the ZnO-PP is nearly half of that achievable on ZnO-SG and higher degradation rate due to the higher value of the rate constants. There are few literatures that have found photocatalytic activity similar to ZnO but, most of them use co-catalysts or dopants to support use of low energy, use supports to enhance surface area or, to use radiation of higher energy [15].

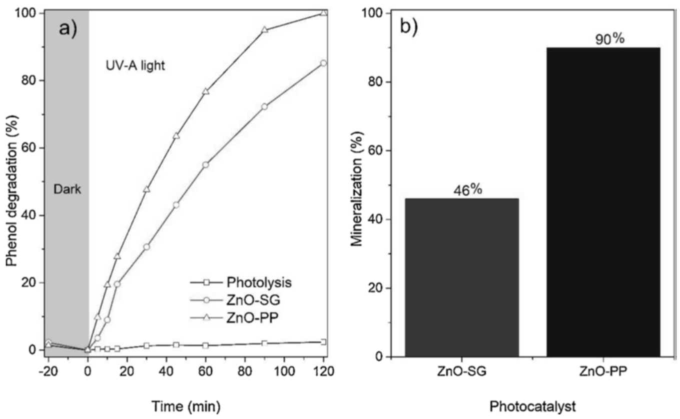

Fig. 6. Qualitative analysis of the data In the current study, the phenol degradation rates utilised in analysis were 110 minutes. b) The determination of the content of TOC after photocatalytic process on water using ZnO nanoparticles applied various synthesis methods

IV. CONCLUSION

Thus, in this paper, we have compared two techniques as the methods for synthesising ZnO nanoparticles. From observation made the preparation method could explain the differences in the characteristic of the NPs such as morphology, particle size, surface area, and the potential. These differences led to generation of hydroxyl radicals in different ways and thus enhanced the photocatalytic performance of ZnO prepared using the precipitation method notwithstanding, sol-gel nanoparticles also demonstrated rather encouraging phenol photodegradation rates as well. This is rather surprising as in general, the ZnOPP exhibited the following characteristics, a larger specific surface area, smaller particle size, slightly higher O/V ratio, and the surface charge of the particles as electropositive compared to the ZnO-SG samples. These properties enhanced the photocatalytic properties of ZnO for the degradation and mineralization of phenol and is thus considered as a stable refractory pollutant. The electrostatic attraction was possible between ZnO-PP NPs and phenol due to the positive surface charge being effective in the aqueous media. Besides, it is also suggested that the fractal dimension, here related to surface roughness of the particles, may affect both: The possible processes include the adsorption of the pollutant molecule and generation of hydroxyl species for which further studies are required. Also significant, and is for that matter the use of precipitation method and the zinc nitrate as the precursors, was the enhanced creation of oxygen vacancies that are important in the generation of hydroxyl radicals using the UVA radiation that is the lower energy type of UV light.

REFERENCES

1) Ghoderao, Karuna P., Shweta N. Jamble, and Rohidas B. Kale. "Influence of pH on hydrothermally derived ZnO nanostructures." Optik 156 (2018): 758-771.
2) Shidpour, Reza, Abdolreza Simchi, Faegheh Ghanbari, and Manouchehr Vossoughi. "Photo-degradation of organic dye by zinc oxide nanosystems with special defect structure: Effect of the morphology and annealing temperature." Applied Catalysis A: General 472 (2014): 198-204.
3) Sliem, Mahmoud A., Ahmed Youssef Salim, and Gehad Genidy Mohamed. "Photocatalytic degradation of anthracene in aqueous dispersion of metal oxides nanoparticles: Effect of different parameters." Journal of Photochemistry and Photobiology A: Chemistry 371 (2019): 327-335.
4) Gnanaprakasam, A., V. M. Sivakumar, P. L. Sivayogavalli, and M. Thirumarimurugan. "Characterization of TiO2 and ZnO nanoparticles and their applications in photocatalytic degradation of azodyes." Ecotoxicology and environmental safety 121 (2015): 121-125.
5) Garrido, Isabel, Marta Pastor-Belda, Natalia Campillo, Pilar Viñas, María José Yañez, Nuria Vela, Simon Navarro, and José Fenoll. "Photooxidation of insecticide residues by ZnO and TiO2 coated magnetic nanoparticles under natural sunlight." Journal of Photochemistry and Photobiology A: Chemistry 372 (2019): 245-253.
6) Adam, Rania E., Gallia Pozina, Magnus Willander, and Omer Nur. "Synthesis of ZnO nanoparticles by co-precipitation method for solar driven photodegradation of Congo red dye at different pH." Photonics and Nanostructures-Fundamentals and Applications 32 (2018): 11-18.
7) Sridar, R., U. Uma Ramanane, and M. Rajasimman. "ZnO nanoparticles–Synthesis, characterization and its application for phenol removal from synthetic and pharmaceutical industry wastewater." Environmental nanotechnology, monitoring & management 10 (2018): 388-393.
8) Noei, Heshmat, Hengshan Qiu, Yuemin Wang, Elke Löffler, Christof Wöll, and Martin Muhler. "The identification of hydroxyl groups on ZnO nanoparticles by infrared spectroscopy." Physical Chemistry Chemical Physics 10, no. 47 (2008): 7092-7097.
9) Muñoz-Hernández, Gerardo, Alejandro Escobedo-Morales, and Umapada Pal. "Thermolytic growth of ZnO nanocrystals: morphology control and optical properties." Crystal Growth and Design 9, no. 1 (2009): 297-300.
10) Zhong, Xinghua, Yaoyu Feng, Yuliang Zhang, Ingo Lieberwirth, and Wolfgang Knoll. "Nonhydrolytic alcoholysis route to morphology‐controlled ZnO nanocrystals." Small 3, no. 7 (2007): 1194-1199.
11) Zak, A. Khorsand, M. Ebrahimizadeh Abrishami, WH Abd Majid, Ramin Yousefi, and S. M. Hosseini. "Effects of annealing temperature on some structural and optical properties of ZnO nanoparticles prepared by a modified sol–gel combustion method." Ceramics International 37, no. 1 (2011): 393-398.
12) Samadipakchin, Parvin, Hamid Reza Mortaheb, and Alireza Zolfaghari. "ZnO nanotubes: Preparation and photocatalytic performance evaluation." Journal of Photochemistry and Photobiology A: Chemistry 337 (2017): 91-99.

13) Omri, Karim, I. Najeh, R. Dhahri, J. El Ghoul, and L. J. M. E. El Mir. "Effects of temperature on the optical and electrical properties of ZnO nanoparticles synthesized by sol–gel method." Microelectronic Engineering 128 (2014): 53-58.
14) Al-Gaashani, R., S. Radiman, A. R. Daud, N. Tabet, and Y. J. C. I. Al-Douri. "XPS and optical studies of different morphologies of ZnO nanostructures prepared by microwave methods." Ceramics International 39, no. 3 (2013): 2283-2292.
15) Rosman, Nurafiqah, Wan Norharyati Wan Salleh, Ahmad Fauzi Ismail, Juhana Jaafar, Zawati Harun, Farhana Aziz, Mohamad Azuwa Mohamed, Bunsho Ohtani, and Mai Takashima. "Photocatalytic degradation of phenol over visible light active ZnO/Ag2CO3/Ag2O nanocomposites heterojunction." Journal of Photochemistry and Photobiology A: Chemistry 364 (2018): 602-612.